PCCP

PAPER

View Article Online
View Journal | View Issue

Cite this: *Phys. Chem. Chem. Phys.*, 2014, **16**, 4807

Bright yellow and green Eu(II) luminescence and vibronic fine structures in $LiSrH_3$, $LiBaH_3$ and their corresponding deuterides†

Nathalie Kunkel,*[a] Andries Meijerink[b] and Holger Kohlmann*[c]

Received 3rd December 2013,
Accepted 13th January 2014

DOI: 10.1039/c3cp55102d

www.rsc.org/pccp

The luminescence of Eu^{2+} in hydride and deuteride perovskite hosts $LiMH_3$ and $LiMD_3$ (M = Sr, Ba) is reported. Bright yellow (M = Sr) and green (M = Ba) emission is observed and assigned to $4f^6 5d–4f^7$ emission from Eu^{2+} in the highly symmetric 12-coordinated M^{2+} site ($m\bar{3}m$). The long wavelength of the emission is explained by the strong covalence and crystal field splitting in europium's coordination by hydride anions. A well-resolved vibrational structure in the emission and excitation spectra of Eu^{2+} in the Sr-compounds allows for an accurate determination of the energy of the lowest $4f^6 5d$ state and vibrational frequencies, for both the hydride and deuteride. The isotope effect on the energy of the fd states is small (~70 cm^{-1}), as expected. Surprisingly, also the vibrational energies observed in the vibronic progression are similar for the d–f emission spectra in $LiSrH_3$ and $LiSrD_3$. This is explained by strong coupling of the d–f emission with low energy acoustic phonons which, contrary to optical phonons, are not strongly affected by replacing H by D. The present results provide insight into the long wavelength Eu^{2+} emission in hydride coordination and the influence of isotope replacement on the luminescence.

Introduction

Due to their high luminescence efficiency, Eu(II) containing host lattices are of great interest for application as luminescent materials (phosphor) in light emitting devices. In the majority of cases, in the spectra of Eu(II) parity-allowed electric dipole transitions ($4f^6 5d^1 \rightarrow 4f^7$) are observed. As the d-electrons are relatively unshielded against interactions with the lattice, the emission energies of these transitions show a strong dependence on the coordination sphere.[1] This leads to typically blue or green emission in oxides, halides, borates and sulfates, and green to orange emission in compounds with more polarizable anions, such as sulfides or nitrides[2–4] with potential application in efficient warm white LEDs.[3] In this regard, Eu(II) coordinating hydride anions promise interesting behavior, because high polarizability and considerable covalence are expected leading to redshifted emission.

Metal hydrides as host lattices for divalent europium form a new class of luminescent materials and so far the only hydride host lattices studied are the alkaline earth metal hydrides.[5] A strong redshift of the emission wavelength was found in MH_2:Eu^{2+} (M = Ca, Sr, Ba), which was attributed to a stronger nephelauxetic effect (higher covalence) of the hydride ligands and also to a larger ligand field of the hydride anion in comparison to fluoride.[5] In these compounds europium has a relatively low site symmetry (m) and coordination number nine. Due to the difference in crystal structure with the fluorides MF_2 a direct comparison with the luminescence of Eu^{2+} in hydrides and fluorides is hampered. In order to widen the understanding of the luminescence of europium in metal hydrides, other coordination numbers and higher symmetries need to be included. To avoid luminescence quenching, host compounds with a sufficiently large bandgap should be chosen, *i.e.* salt-like compounds like the ionic alkaline and alkaline earth hydrides. Several ternary compounds are known within this class, *e.g.* the perovskites $LiMH_3$ (M = Sr,[6] Ba,[7] Eu[8]) and the structurally diverse group of ternary alkaline or alkaline earth magnesium hydrides.[9] Analogous europium compounds exist in many cases, in which europium is always in its divalent state.[10] Europium is likely to replace alkaline earth metals in their hydrides and in some cases solid solutions of europium and alkaline earth hydrides have been realized.[11,12] Salt-like alkaline earth metal hydrides therefore seem to be good potential hosts for Eu^{2+}.

In this work we investigate the luminescence properties of Eu(II) in the inverse perovskites $LiSrH_3$:Eu^{2+} (0.5 mol%) and $LiBaH_3$:Eu^{2+} (0.5 mol%) and their corresponding deuterides.

[a] *Inorganic and Solid State Chemistry, Saarland University, P.O. Box 151150, 66041 Saarbrücken, Germany. E-mail: n.kunkel@mx.uni-saarland.de*
[b] *Debye Institute, Utrecht University, P.O. Box 80 000, 3508 TA Utrecht, Netherlands*
[c] *Inorganic Chemistry, University Leipzig, Johannisallee 29, 04103 Leipzig, Germany. E-mail: holger.kohlmann@uni-leipzig.de*

† Electronic supplementary information (ESI) available: Experimental details and detailed luminescence spectra. See DOI: 10.1039/c3cp55102d

Europium is expected to be divalent and occupy the high symmetry site ($m\bar{3}m$) of the alkaline earth metal. It is surrounded by twelve hydrogen or deuterium atoms in a cubooctahedral arrangement of the perovskite structure. This structure type has been unambiguously confirmed for $LiBaH_3$, $LiBaD_3$[7] and $LiEuD_3$,[8] so far. Sr–H and Eu–H distances are typically about 10 pm larger for coordination number twelve as compared to coordination number nine.[13] The corresponding fluoroperovskite $LiBaF_3:Eu^{2+}$ has been studied before[14] and is isostructural. This allows for a direct comparison of the Eu^{2+} emission in isostructural fluorides and hydrides and will give a better understanding of the origin of the red shift observed for d–f emission in hydrides. The strontium compound does not feature a corresponding fluoride compound.[15] Both hydride and deuteride compounds are investigated to study a possible isotope effect on the luminescence. Studies on isotope effects are limited for lanthanide luminescence to very subtle effects on f–f transition.[16,17] No strong influence is expected on the position of energy levels due to a similar covalence and ligand field for H^- and D^-. Vibrational energies are expected to be higher in the hydrides due to the lower effective mass.

Materials and methods

The metal hydrides were obtained by hydrogenation of the corresponding alloys and structures were characterized *via* X-ray powder diffraction. In order to clarify that the compounds crystallize in the cubic inverse perovskite structure type, neutron powder diffraction data for $LiSrH_3$ and $LiBaH_3$ were collected at the D20/ILL/Grenoble (for details see ESI†).

Photoluminescence emission and absorption spectra were measured on an Edinburgh Instruments FLS920 spectrofluorometer equipped with a double monochromator (Czerny-Turner, 300 mm focal length) for the excitation beam, a monochromator for UV/Vis detection and a 450 W Xenon lamp for sample excitation. For detection, a photomultiplier tube R928P (Hamamatsu) was used. For low temperature measurements an Oxford liquid helium flow cryostat was used. Luminescence decay curves were measured under pulsed excitation using an Edinburgh 376.8 nm pulsed diode laser (65 ps pulses). Samples were enclosed in sealed silica tubes of 0.5–1 mm diameter. Luminescence decay curves were analyzed using a single exponential function, even though in the higher temperature range a small deviation from single exponential was observed (faster initial decay).

Results and discussion

$LiSrH_3:Eu^{2+}$ and $LiSrD_3:Eu^{2+}$

Both $LiSrH_3:Eu^{2+}$ and $LiSrD_3:Eu^{2+}$ (0.5 mol%) show an intense yellow luminescence under UV excitation (Fig. 1). The europium-free sample $LiSrH_3$ does not exhibit any visible luminescence demonstrating that the bright yellow emission originates from Eu^{2+}.

Crystallography

In the cubic perovskite $A^IM^{II}X_3$ the M atoms are octahedrally coordinated by X atoms, while A atoms have twelve X neighbors in a cubooctahedral arrangement. In the *inverse* cubic perovskite type, the positions of A and M atoms are interchanged (Fig. 2). Due to the low scattering power of hydrogen for X-rays the two varieties of the cubic perovskite are indistinguishable and neutron diffraction is needed to differentiate between normal and *inverse* cubic perovskites. Our neutron powder diffraction experiments show unambiguously that $LiSrH_3$ crystallizes in the *inverse* perovskite structure type (Fig. 2, space group type $Pm\bar{3}m$; for neutron powder diffraction data see Fig. S1 of the ESI†).

Assuming a statistical occupation of the strontium site 1(b) by europium and strontium, the following interatomic distances were obtained from X-ray powder diffraction data (Table 1).

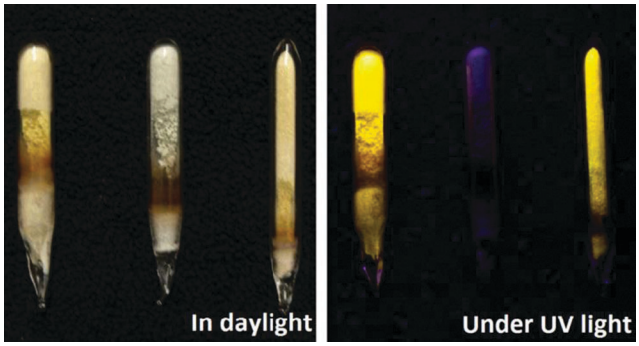

Fig. 1 From left to right: $LiSrD_3:Eu^{2+}$, $LiSrH_3$ and $LiSrH_3:Eu^{2+}$ sealed in silica ampoules at daylight and under UV excitation (360 nm).

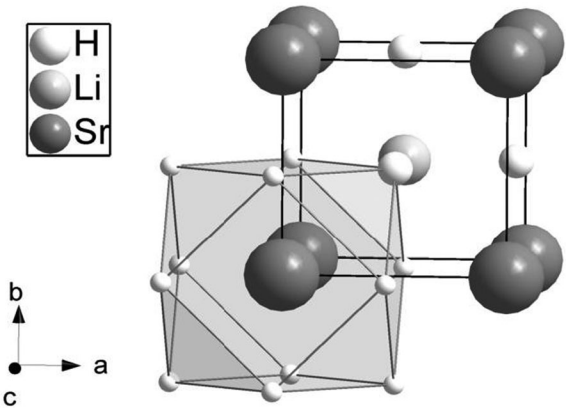

Fig. 2 The crystal structure of $LiSrH_3$ showing the cubooctahedral surroundings of strontium (site symmetry $m\bar{3}m$) with hydrogen. The corresponding barium and europium compounds are isotopic[8,9] in the inverse cubic perovskite type.

Luminescence spectra

Luminescence spectra recorded at room temperature exhibit broad excitation and emission bands which are assigned to parity-allowed electric dipole transitions between the $4f^7$ and $4f^65d$ levels of Eu^{2+}. In Fig. 3 and 4 the temperature dependent emission spectra of $LiSrH_3:Eu^{2+}$ and $LiSrD_3:Eu^{2+}$ are shown at an excitation wavelength of 360 nm.

At room temperature broad emission bands are observed at around ~570 nm. Below 80 K, the spectra of $LiSrH_3:Eu^{2+}$ (below 50 K in the case of $LiSrD_3:Eu^{2+}$) start showing a

Table 1 Lattice parameters and interatomic distances in $LiSrH_3$:Eu^{2+} and $LiSrD_3$:Eu^{2+} (0.5 mol%) (in pm) at 293(1) K. ($LiSrH_3$ a = 383.572(4))

$LiSrH_3$:Eu^{2+} a = 383.498(3)	
Eu/Sr–H	271.174(2)
Li–H	191.749(2)
$LiSrD_3$:Eu^{2+} a = 382.535(3)	
Eu/Sr–D	270.493(2)
Li–D	191.267(2)

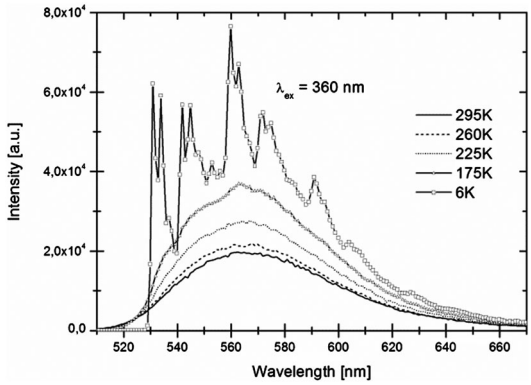

Fig. 3 Temperature-dependent emission spectra of $LiSrH_3$:Eu^{2+} (0.5 mol%) for 360 nm excitation. Intensities increase with decreasing temperatures.

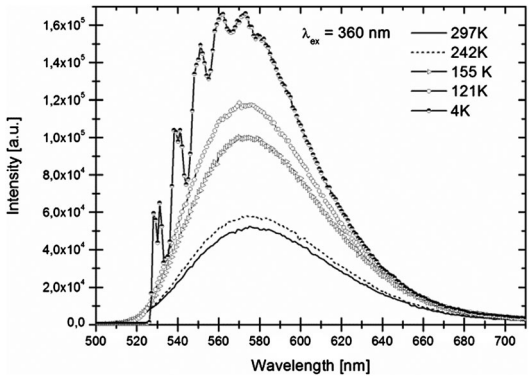

Fig. 4 Temperature-dependent emission spectra of $LiSrD_3$:Eu^{2+} (0.5 mol%) for 360 nm excitation. Intensities increase with decreasing temperatures.

vibrational fine structure. For the hydride the vibronic structure is more pronounced and the individual vibronic lines are better resolved than for the deuteride. Below the vibronic structure will be discussed in detail. Emission intensities decrease above 120 K and are generally about three times higher for the deuteride compared to the hydride, although an accurate quantitative comparison is hampered by alignment differences for the ampoules.

In Fig. 5 details of the emission spectra of $LiSrH_3$:Eu^{2+} at 4 K are depicted. In the range of 450 to 550 nm vibrational fine structure is also visible in the excitation spectra (see Fig. 6). The observation of vibrational fine structure is typical for intermediate coupling strength of electronic transitions with vibrations.

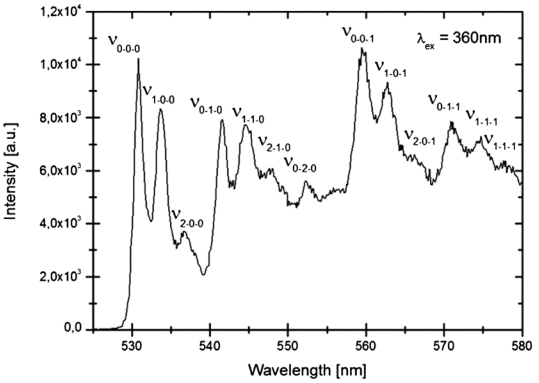

Fig. 5 Higher resolution emission spectrum of $LiSrH_3$:Eu^{2+} (0.5 mol%) at 4 K, excitation at 360 nm. The zero-phonon line (0–0–0) and vibronic replicas (ν_{x-y-z}) are indicated and discussed in the text.

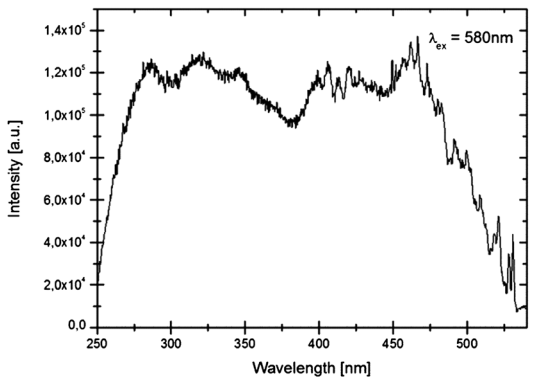

Fig. 6 Excitation spectrum of $LiSrH_3$:Eu^{2+} (0.5 mol%) at 4 K, emission at 580 nm.

A careful analysis of the vibronic structure reveals valuable information on the electron–phonon coupling strength and the phonon energies. The vibronic pattern is well-resolved and complex, involving coupling with at least three different vibrations. In Table 2 the energies of the vibronic lines with respect to the zero-phonon (labeled 0−0−0) line are tabulated for the Eu^{2+} emission and excitation spectrum in $LiSrH_3$ and $LiSrD_3$. A typical pattern of three closely spaced lines $\sim$100 cm^{-1} apart is repeated at $\sim$370 cm^{-1} intervals. This can be explained by coupling of the $4f^6$5d transition with vibrations of these two energies. In the assignment in Fig. 6 of the vibronic lines with ν_{x-y-z} the number x indicates the vibronic replica of the lower energy $\sim$100 cm^{-1} vibration and the number y the $\sim$370 cm^{-1} vibration. The pattern for the 100 cm^{-1} vibration shows a strong 0–x line and weaker 1–x and 2–x lines, typical for a Huang–Rhys coupling parameter S around 0.8. The ratio between the 0–0 line and vibronic replicas n can be calculated from:[18]

$$I_n = e^{-S}\,(S^n/n!)$$

For a Huang–Rhys coupling parameter S of 0.8 a ratio of 0.8 is expected for the 0–1/0–0 intensity, close to the experimentally observed ratio for the 100 cm^{-1} phonon replica. The intensity variation for the vibronic lines of the 350 cm^{-1}

Table 2 Vibronics in the excitation and emission spectrum at 4 K for the $4f^6 5d - {}^8S_{7/2}$ transition of Eu^{2+} in $LiSrH_3:Eu^{2+}$ and $LiSrD_3:Eu^{2+}$ (0.5 mol%). ΔE gives the energy of the vibrational modes with respect to their zero phonon lines. Assignments in the left columns are for the vibronic lines observed in the emission spectra

	$LiSrH_3:Eu^{2+}$		$LiSrD_3:Eu^{2+}$
Line	ΔE [cm^{-1}]	Line	ΔE [cm^{-1}]
Emission			
ν_{1-0-0}	99	ν_{1-0}	96
ν_{2-0-0}	204	ν_{2-0}	198
ν_{0-1-0}	374	ν_{0-1}	338
ν_{1-1-0}	476	ν_{1-1}	420
ν_{2-1-0}	591	ν_{2-1}	542
ν_{0-2-0}	730		
ν_{0-0-1}	964		
ν_{1-0-1}	1068		
ν_{2-0-1}	1195		
ν_{0-1-1}	1324		
ν_{1-1-1}	1424		
ν_{2-1-1}	1532		
Excitation			
ν_{1-0-0}	93	ν_{1-0}	86
ν_{2-0-0}	194	ν_{2-0}	123
ν_{0-1-0}	362	ν_{0-1}	225
ν_{1-1-0}	451	ν_{1-1}	336
ν_{2-1-0}	495	ν_{2-1}	440
ν_{0-2-0}	548		
ν_{0-0-1}	692		
ν_{1-0-1}	784		
ν_{2-0-1}	908		
ν_{0-1-1}	1057		
ν_{1-1-1}	1161		
ν_{2-1-1}	1322		

vibration (0–0–0, 0–1–0) shows a stronger 0–0 line and a weaker 1–0 line with a ratio of ~0.7 indicating that S is around 0.7 for this vibrational mode. Due to the uncertainty in the background, it is difficult to accurately determine S. At 964 cm^{-1} another strong line is observed with replicas at ~100 cm^{-1} intervals. This indicates coupling to a third vibrational mode at ~970 cm^{-1}. In addition to the replicas at 100 cm^{-1} and at 370 cm^{-1} a group of three lines at 100 cm^{-1} is observed, which can be assigned to vibronic overtones due to coupling with all three vibrations (970 cm^{-1}, 380 cm^{-1} and 100 cm^{-1}). For the 970 cm^{-1} vibration S is similar, approximately 0.7. In Table 2 all lines are assigned to ν_{x-y-z} where x, y and z indicate the number of vibrations involved in the 100 cm^{-1} (x), 370 cm^{-1} (y) and 970 cm^{-1} (z) vibrations. It is rare that d–f emission spectra of lanthanides show such a well-resolved vibrational fine structure in which multiple vibrational modes can be identified. In previous work well-resolved spectra showing coupling with two vibrations have been reported for Ce^{3+}, Pr^{3+} and Tb^{3+} in elpasolites[18–20] with values for S between 1 and 2.

The excitation spectra also show clear vibronic features, similar to those observed in the emission spectra. The vibrational features observed in Fig. 6 are shown in more detail in the ESI† (Fig. S2). The observation of vibronic structure is complicated by the fact that the $4f^6 5d$ excited state is split into multiple electronic states due to the splitting of the $4f^6$ configuration in ^7F_J levels.[21] The splitting of these levels is of the same order as the vibrational energies (100–1000 cm^{-1}) which complicates the analysis of the vibronic structure. The low energy vibrations can be however clearly observed. At 93 cm^{-1} and 362 cm^{-1} from the 0–0 line vibronic side bands are observed, with a relative intensity of ~0.8. These lines are assigned to the same vibrational modes as the 99 cm^{-1} and 374 cm^{-1} vibrations observed in the emission spectra. It interesting to note that the vibrational energies in the emission spectra (ground state vibrations) are slightly higher than those in the excitation spectra (excited state vibrations). Higher vibrational energies imply a higher force constant and thus stronger bonding in the ground state of Eu^{2+} compared to the excited state. Recent experimental[18] and theoretical work[22] has shown that the bonding in the $4f^6 5d$ excited state can be stronger or weaker than in the ground state, depending on the 5d orbital (e_g or t_{2g} in cubic coordination). Experimental evidence and *ab initio* calculations have provided evidence for a weaker bonding in the $5d(e_g)$ state and stronger bonding in the $5d(t_{2g})$ state. The lowest 5d-state in cubic 12-coordination has e_g symmetry and the presently found results are consistent with a weakening of the Eu–ligand bond for the $4f^6 5d(e_g)$ excited state.

The low temperature emission spectrum of Eu^{2+} in the deuteride shows a well-resolved vibrational structure, although not as clear as for the hydride. A higher resolution emission and excitation spectrum showing the vibronic features is included in the ESI† (Fig. S3 and S4). The energies of the vibronic lines relative to the zero-phonon line deduced from these spectra are tabulated in Table 2. Two vibrational modes can be clearly distinguished in the emission spectrum, a 96 cm^{-1} and a 340 cm^{-1} vibrational mode. The Huang–Rhys parameter for the 96 cm^{-1} mode is ~0.9, for the 340 cm^{-1} mode it seems to be higher but it is difficult to determine due to the strong background. In the excitation spectrum the low energy vibration is 86 cm^{-1}, lower in energy than the corresponding ground state vibrational mode observed in the emission spectrum. This is consistent with a weaker bonding in the $4f^6 5d(e_g)$ excited state.

It is interesting to study the influence of replacing H with D. In view of the similar chemical properties, the covalence and ligand field splitting are expected to be similar in $LiSrH_3$ and $LiSrD_3$. The position of the lowest $4f^6 5d$ states is similar for Eu^{2+} in the hydride and deuteride (zero-phonon line at 531 nm in the hydride and 529 nm in the deuteride). The small shift of ~70 cm^{-1} can be related to the small difference in lattice parameters. The difference in the vibrational energies observed in the vibronic structure for Eu^{2+} in the hydride and deuteride is also rather small, with slightly (5–10%) higher energies for the hydride. This is unexpected. Typically a strong influence is observed upon replacing H with D. The two times higher mass of D gives a $\sqrt{2}$ reduction of the vibrational energy. Previous research has shown that for the high energy optical phonons the expected $\sqrt{2}$ dependence is observed. However, the low energy (50–300 cm^{-1}) acoustic phonons were shown to be very similar for metal hydrides and deuterides.[23,24] The low-energy phonon modes observed in the well-resolved progression are thus assigned to acoustic phonons. The broad background at higher energies will have a contribution of higher energy optical phonons.

Furthermore, we estimate the crystal field splitting for the cubooctahedral field between $4f^7 5d(e_g)$ and $4f^7 5d(t_{2g})$ to be approx. 7800 cm^{-1} for both hydride and deuteride. The splitting is estimated from the position of the zero-phonon line (~530 nm) and the onset of the $4f^6 5d(t_{2g})$ excitation band at around 375 nm. An accurate determination is difficult due to uncertainty in the position of the onset of the $4f^6 5d(t_{2g})$ excitation band.

Luminescence lifetimes were recorded as a function of temperature. Close to single exponential decay curves were obtained (see also ESI†) at low temperatures. At room temperature the decay cures deviate from a single exponential. Emission lifetimes at low temperatures are about 420 ns for the hydride and 450 ns for the deuteride. This is somewhat shorter than expected for decay times for parity-allowed transitions between the $4f^6 5d$ excited state and the $^8S_{7/2}$ ($4f^7$) ground state given in (24). Typically, a decay time of around 1 to 1.4 μs is expected for Eu^{2+} emission at around 560 nm.[25] The reason for the short decay time is probably the high refractive index n of hydrides. The refractive index of most oxides in which yellow Eu^{2+} emission has been observed is ~1.6. For hydrides n is ~2.[26] The refractive index has a strong influence on the radiative decay rate and increase of n from 1.6 to 2 will be more than double the radiative decay rate, consistent with the two times faster decay observed for Eu^{2+} emission in the hydrides compared to oxides.

The temperature dependence of the decay times shows that the emission quenches above ~150 K (Fig. 7) which is also observed in the temperature dependent emission spectra in Fig. 3 and 4. Temperature quenching can have different origins. In the configuration coordinate model temperature is explained by thermally activated cross-over from the excited state to the ground state. In this model the quenching temperature is expected to be strongly correlated with S. Strong electron–phonon coupling (large S) is related to lower quenching temperatures. The Eu^{2+} emission in $LiSrH_3$ and $LiSrD_3$ is characterized by weak electron–phonon coupling ($S \sim 1$, small Stokes shift and a narrow emission band) which rules out thermally activated cross-over as the quenching mechanism for the Eu^{2+} emission in $LiSrH_3$ and $LiSrD_3$. The alternative mechanism is thermally activated photoionization. If the emitting $4f^6 5d$ state is situated just below the conduction band, thermally activated ionization from the $4f^6 5d$ excited state to the conduction band quenches the emission. The small bandgap of hydrides[27] is in line with the $4f^6 5d$ state situated just below the conduction band and makes thermally activated photoionization the more probable quenching mechanism.

$LiBaH_3:Eu^{2+}$ and $LiBaD_3:Eu^{2+}$

$LiBaH_3:Eu^{2+}$ and $LiBaD_3:Eu^{2+}$ (0.5 mol%) show an intense green emission (see Fig. 8).

Crystallography

Neutron powder diffraction experiments show that $LiBaH_3$ crystallizes in the inverse perovskite structure, thus confirming earlier results on $LiBaH_3$ and $LiBaD_3$.[7] For the distances given in Table 3, a statistical occupation of the barium site 1(b) by europium and barium was assumed. Just as for the Sr-compounds, slightly smaller distances are obtained for the deuterides.

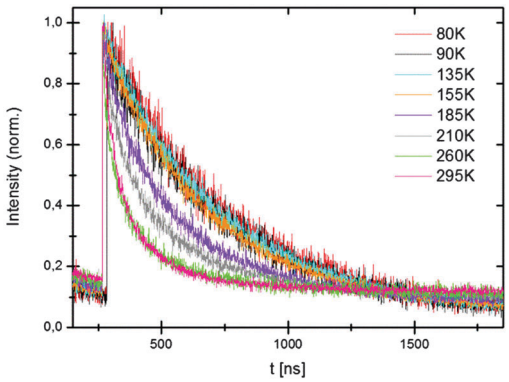

Fig. 7 Temperature dependence of the decay curves of $LiSrD_3:Eu^{2+}$ (0.5 mol%); emission at 580 nm.

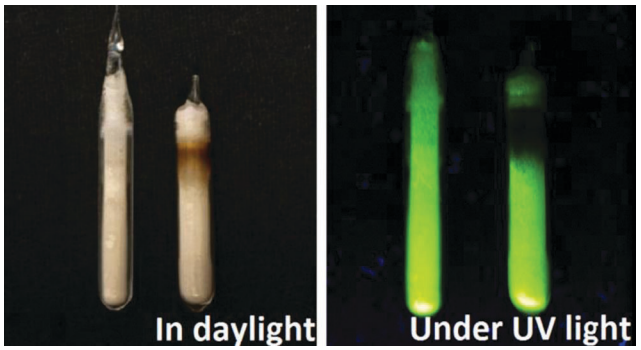

Fig. 8 From left to right: $LiBaD_3:Eu^{2+}$ and $LiBaH_3:Eu^{2+}$ sealed in silica ampoules at daylight and under UV excitation (360 nm).

Table 3 Lattice parameters and interatomic distances in $LiBaH_3:Eu^{2+}$ and $LiBaD_3:Eu^{2+}$ (0.5 mol%) (in pm) at 193(1) K ($LiBaH_3$ a = 402.395(2))

$LiBaH_3:Eu^{2+}$ a = 402.284(3)	
Eu/Ba–H	284.458(2)
Li–H	201.142(2)
$LiBaD_3:Eu^{2+}$ a = 401.459(3)	
Eu/Ba–D	283.750(2)
Li–D	200.730(2)

Luminescence spectra

In Fig. 9 the emission spectrum of Eu^{2+} in $LiBaH_3$ is shown. A broad emission band with a maximum at around 530 nm, in the green spectral region, is observed at room temperature.

With decreasing temperature, intensities first increase slightly, but then below approx. 130 K show a significant decrease. Below 65 K, the spectra of $LiBaH_3:Eu^{2+}$ (50 K in the case of $LiBaD_3:Eu^{2+}$) show a vibrational fine structure, which is, however, not as well-resolved as for the strontium compounds. As for the strontium compounds, emission intensities of the deuteride are higher than for the hydride but an accurate quantitative comparison is difficult, as discussed before, for

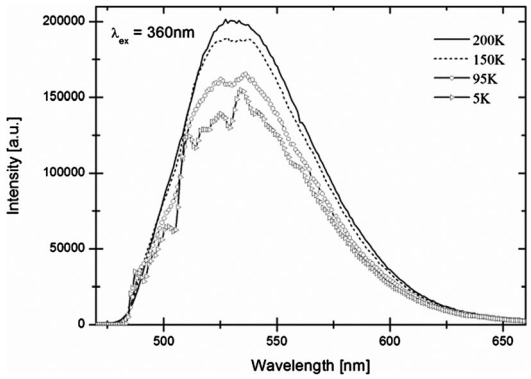

Fig. 9 Temperature-dependent luminescence spectra of $LiBaH_3:Eu^{2+}$ (0.5 mol%).

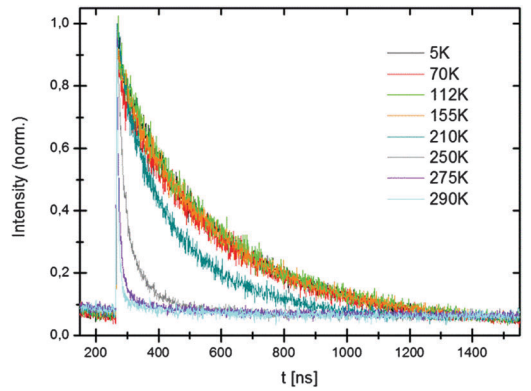

Fig. 10 Temperature dependence of the decay curves of $LiBaH_3:Eu^{2+}$ (0.5 mol%) emission at 550 nm.

luminescent materials in ampoules. Due to the less well-resolved vibrational structure only a few vibrational energies can be determined (for vibrational energies see Table S1 of the ESI†).

Lifetimes at low temperatures and 550 nm are about 295 ns for the hydride and 280 ns for the deuteride. The luminescence lifetimes are shorter than for the Eu^{2+} in the Sr-compounds and this is partly due to the shorter emission wavelength (530 nm *vs.* 570 nm). Based on the λ^3 dependence of the luminescence lifetime a 1.25 shorter lifetime is expected. The temperature dependence of the decay times (see Fig. 10) shows a decrease of the lifetimes at temperatures above 200 K which is due to luminescence quenching. Just as for the Sr-hydrides, the quenching is attributed to thermally activated photoionization.

Discussion

To gain insight into the factors determining the red shift of the emission in hydrides in comparison to fluorides, it is important to separate the contribution due to the nephelauxetic effect (covalence) and crystal field splitting. Since $LiBaF_3$, $LiBaH_3$ and $LiSrH_3$ all have the same perovskite structure a meaningful comparison can be made. In Table 4 information obtained from the spectra is collected. The crystal field splitting is determined from the onset of the low energy $4f^65d$ excitation band (zero-phonon line in the excitation spectrum) and the onset of the second excitation band ($4f^65d(t_{2g})$) observed in the excitation spectrum. The barycenter of the $4f^65d$ state is the degeneracy weighted average of the two $4f^65d$ states. The data show that the large redshift of the $4f^65d$ emission is primarily caused by the strong nephelauxetic effects of the covalent hydride ligands, shifting the barycenter of the $4f^65d$ state to some 10 000 cm^{-1} lower energy. Also the larger crystal field splitting contributes to a red shift but the influence is ten times smaller. For comparison, the zero-phonon line of the Eu^{2+} $4f^7(^6P_{7/2})$ to $4f^7(^8S_{7/2})$ intraconfigurational transition is located at 27 535 cm^{-1} in BaFCl and the transition from the lowest $4f^65d$ state to the $4f^7(^8S_{1/2})$ ground state near 26 000 cm^{-1}, respectively.[28]

Table 4 Comparison of spectroscopic properties of the $4f^65d$ states of Eu^{2+} in fluoride and hydride perovskites

	$LiBaF_3:Eu^{2+}$	$LiBaH_3:Eu^{2+}$	$LiSrH_3:Eu^{2+}$
Onset e_g (nm)	335	485	530
Onset t_{2g} (nm)	275	355	375
Crystal field splitting (cm^{-1})	6500	7500	7800
Barycenter (cm^{-1})	33 760	25 150	23 550

Conclusion

Hydrides doped with Eu^{2+} form an exciting class of luminescent materials with a long wavelength $4f^65d$ emission. Here we have investigated Eu^{2+} luminescence in $LiMH_3$ and $LiMD_3$ (M = Sr, Ba) and observed a bright yellow (M = Sr) and green (M = Ba) $4f^65d$ emission. For Eu^{2+} luminescence in the strontium compounds a well-resolved vibrational fine structure is observed in both the emission and excitation spectra. The complex vibronic structure can be explained by coupling with three vibrational modes of ~100, ~370 and ~970 cm^{-1} with a small Huang Rhys phonon coupling parameter S of 0.7–1 for the different vibrations. Comparison of the vibrational energies in emission and excitation spectra reveals a 5–10% higher energy for the emission spectra, indicating a stronger bonding in the $4f^7$ ground state compared to the $4f^65d(e_g)$ excited state, in line with recent *ab initio* calculations. For the deuterides the vibrational frequencies are slightly smaller than for the hydrides, but less than expected for the large change in effective mass. The small change indicates that vibronic lines observed in the emission spectra originate from coupling with acoustic phonons which are less affected by the D–H isotope substitution.

For Eu^{2+} in the $LiBaH_3$ a bright green emission is observed. The radiative lifetime of the Eu^{2+} $4f^65d$ emission in the hydrides and deuterides is 300–400 ns, shorter than observed in oxide and halide hosts. The short emission lifetime is explained by the high refractive index of hydrides. Analysis of the spectra reveals that the large redshift observed for Eu^{2+} $4f^65d$ emission in hydrides is largely due to the strong nephelauxetic effects of the hydride ligands which shifts the barycenter of the $4f^65d$ state to some 10 000 cm^{-1} lower energy in comparison with isostructural fluorides. The larger crystal field splitting for

hydride coordination has a small ($\sim$1000 cm^{-1}) contribution to the red shift of the emission. The present results on the 4f^{6}5d emission of Eu^{2+} in hydrides have provided new insights that further the understanding of this class of luminescent materials. Based on the high symmetry and detailed information from the well-resolved vibrational fine structure, $LiSrH_3$:Eu^{2+} and $LiBaH_3$:Eu^{2+} are very suitable as model systems for theoretical (*ab initio*) calculations to better understand excited 4f^{n-1}5d states of lanthanides.

Funding sources

We are grateful to the Deutsche Forschungsgemeinschaft (DFG) for financial support (grants KO1803/3-1 and KO1803/7-1) and the Landesgraduiertenförderung (LGF) Saarland for a PhD research fellowship.

Acknowledgements

Dr Robert Haberkorn is acknowledged for taking the photographs shown and Prof. Michael Springborg for insightful discussions.

Notes and references

1 P. Dorenbos, *J. Lumin.*, 2003, **104**, 239.
2 P. Dorenbos, *J. Phys.: Condens. Matter*, 2003, **15**, 575.
3 H. Höppe, *Angew. Chem., Int. Ed.*, 2009, **48**, 3572.
4 M. Zeuner, S. Pagano and W. Schnick, *Angew. Chem.*, 2011, **123**, 7898.
5 N. Kunkel, H. Kohlmann, A. Sayede and M. Springborg, *Inorg. Chem.*, 2011, **50**, 5873.
6 C. E. Messer, J. Eastman, R. G. Mers and A. J. Maeland, *Inorg. Chem.*, 1964, **3**, 776.
7 A. J. Maeland and A. F. Andresen, *J. Chem. Phys.*, 1968, **48**, 4660.
8 H. Kohlmann and K. Yvon, *J. Alloys Compd.*, 2000, **299**, L16.
9 K. Yvon and B. Bertheville, *J. Alloys Compd.*, 2006, **425**, 101.
10 H. Kohlmann, *Eur. J. Inorg. Chem.*, 2010, 2582.
11 H. Kohlmann, R. O. Moyer Jr., T. Hansen and K. Yon, *J. Solid State Chem.*, 2003, **174**, 35.
12 H. Kohlmann, K. Yvon and Y. Wang, *J. Alloys Compd.*, 2005, **393**, 11.
13 K. Yvon, H. Kohlmann and B. Bertheville, *Chimia*, 2001, **55**, 505.
14 A. Meijerink, *J. Lumin.*, 1993, **55**, 125.
15 A. J. Maeland and W. D. Lahar, *Z. Phys. Chem.*, 1993, **179**, 181.
16 M. N. Popova, S. A. Klimin, E. P. Chukalina, G. N. Zhizhin, S. L. Korableva and R. Yu Abdulsabirov, *Opt. Spectrosc.*, 2004, **97**, 50.
17 L. Van Pieterson, R. P. A. Dullens, P. S. Peijzel and A. Meijerink, *J. Chem. Phys.*, 2001, **115**, 9393.
18 A. P. Tanner, C. S. K. Mak, N. M. Edelstein, K. M. Murdoch, G. Liu, J. Huang, L. Seijo and Z. Barandiarán, *J. Am. Chem. Soc.*, 2003, **125**, 13225.
19 C. K. Duan, P. A. Tanner, A. Meijerink and V. Makhov, *J. Phys. Chem. A*, 2011, **115**, 9188.
20 L. Ning, C. S. K. Mak and P. A. Tanner, *Phys. Rev. B: Condens. Matter Mater. Phys.*, 2005, **72**, 085127.
21 S. Lizzo, A. H. Velders, A. Meijerink, G. J. Dirksen and G. Blasse, *J. Lumin.*, 1996, **65**, 303.
22 Z. Barandiarán, N. M. Edelstein, B. Ordejón, F. Ruipérez and L. Seijo, *J. Solid State Chem.*, 2005, **178**, 464.
23 H. Dammak, E. Antoshchenkova, M. Hayoun and F. Finocchi, *J. Phys.: Condens. Matter*, 2012, **24**, 435402.
24 A. C. Ho, R. C. Hanson and A. Chizmeshya, *Phys. Rev. B: Condens. Matter Mater. Phys.*, 1997, **55**, 14818.
25 S. H. M. Poort, A. Meijerink and G. Blasse, *J. Phys. Chem. Solids*, 1997, **58**, 1451.
26 A. H. Reshak, M. Y. Shalaginov, Y. Saeed, I. V. Kityk and S. Auluck, *J. Phys. Chem. B*, 2011, **115**, 2836.
27 T. Sato, D. Noréus, H. Takesita and U. Häussermann, *J. Solid State Chem.*, 2005, **178**, 3381.
28 G. K. Liu, X. Y. Chen and J. Huang, *Mol. Phys.*, 2003, **101**, 1029.